MICROWAVE LABORATORY REPORT NO. 87-P-2

FINITE ELEMENT ANALYSIS OF SLOW-WAVE SCHOTTKY CONTACT PRINTED LINES

TECHNICAL REPORT

CHING-KUANG C. TZUANG, DEAN P. NEIKIRK AND TATSUO ITOH

FEBRUARY 16, 1987

AIR FORCE OFFICE OF SCIENTIFIC RESEARCH

GRANT AFOSR-86-0036

UNIVERSITY OF TEXAS
DEPARTMENT OF ELECTRICAL ENGINEERING
AUSTIN, TEXAS 78712

APPROVED FOR PUBLIC RELEASE
DISTRIBUTION UNLIMITED

SECURITY CLASSIFICATION OF THIS PAGE

REPORT DOCUMENTATION PAGE

1a. REPORT SECURITY CLASSIFICATION: UNCLASSIFIED	1b. RESTRICTIVE MARKINGS: AD-A178 259
2a. SECURITY CLASSIFICATION AUTHORITY	3. DISTRIBUTION / AVAILABILITY OF REPORT: unlimited
2b. DECLASSIFICATION / DOWNGRADING SCHEDULE	
4. PERFORMING ORGANIZATION REPORT NUMBER(S): Microwave Laboratory Report No. 87-P-2	5. MONITORING ORGANIZATION REPORT NUMBER(S): AFOSR-TR- 87-0481
6a. NAME OF PERFORMING ORGANIZATION: University of Texas; 6b. OFFICE SYMBOL (If applicable):	7a. NAME OF MONITORING ORGANIZATION: AFOSR
6c. ADDRESS (City, State, and ZIP Code): Department of Electrical & Computer Engineering, University of Texas, Austin, TX 78712	7b. ADDRESS (City, State, and ZIP Code): Bolling AFB, Wash DC 20332
8a. NAME OF FUNDING / SPONSORING ORGANIZATION: AFOSRINE; 8b. OFFICE SYMBOL (If applicable):	9. PROCUREMENT INSTRUMENT IDENTIFICATION NUMBER: AFOSR-86-0036
8c. ADDRESS (City, State, and ZIP Code): Building 410, Bolling AFB, DC 20332-6448	10. SOURCE OF FUNDING NUMBERS: PROGRAM ELEMENT NO. 61102F; PROJECT NO. 2305; TASK NO. C 1; WORK UNIT ACCESSION NO.

11. TITLE (Include Security Classification)

FINITE ELEMENT ANALYSIS OF SLOW-WAVE SCHOTTKY CONTACT PRINTED LINES

12. PERSONAL AUTHOR(S)

CHING-KUANG C. TZUANG, DEAN P. NEIKIRK AND TATSUO ITOH

13a. TYPE OF REPORT	13b. TIME COVERED	14. DATE OF REPORT (Year, Month, Day)	15. PAGE COUNT
technical report	FROM 01 NOV 85 TO 01 NOV 86	Feb. 16, 1987	45

16. SUPPLEMENTARY NOTATION

17. COSATI CODES			18. SUBJECT TERMS (Continue on reverse if necessary and identify by block number)
FIELD	GROUP	SUB-GROUP	

19. ABSTRACT (Continue on reverse if necessary and identify by block number)

Extensive finite element analyses on MMIC (monolithic microwave integrated circuit) slow-wave structures with both localized and layered models are presented. Good agreement is achieved for results obtained in this paper with other theoretical results and experiments. Higher order elements that improve accuracy are discussed. The comparative studies for the Schottky contact microstrip and the coplanar waveguide with localized and layered models are presented. Potential applications of the localized models to more general and practical slow-wave circuits are also discussed.

20. DISTRIBUTION / AVAILABILITY OF ABSTRACT: ☒ UNCLASSIFIED/UNLIMITED ☐ SAME AS RPT. ☐ DTIC USERS	21. ABSTRACT SECURITY CLASSIFICATION: UNCLASSIFIED
22a. NAME OF RESPONSIBLE INDIVIDUAL: W. HT	22b. TELEPHONE (Include Area Code): 767-4931; 22c. OFFICE SYMBOL: NE

DD FORM 1473, 84 MAR — 83 APR edition may be used until exhausted. All other editions are obsolete.

SECURITY CLASSIFICATION OF THIS PAGE

MICROWAVE LABORATORY REPORT NO. 87-P-2

FINITE ELEMENT ANALYSIS OF SLOW-WAVE SCHOTTKY CONTACT PRINTED LINES

TECHNICAL REPORT

CHING-KUANG C. TZUANG, DEAN P. NEIKIRK AND TATSUO ITOH

FEBRUARY 16, 1987

AIR FORCE OFFICE OF SCIENTIFIC RESEARCH

GRANT AFOSR-86-0036

UNIVERSITY OF TEXAS

DEPARTMENT OF ELECTRICAL ENGINEERING

AUSTIN, TEXAS 78712

Finite Element Analysis of Slow-Wave Schottky Contact Printed Lines

Abstract

Extensive finite element analyses on MMIC (monolithic microwave integrated circuit) slow-wave structures with both localized and layered models are presented. Good agreement is achieved for results obtained in this paper with other theoretical results and experiments. Higher order elements that improve accuracy are discussed. The comparative studies for the Schottky contact microstrip and the coplanar waveguide with localized and layered models are presented. Potential applications of the localized models to more general and practical slow-wave circuits are also discussed.

TABLE OF CONTENTS

LIST OF TABLES

LIST OF FIGURES

CHAPTER 1 : Introduction

The advance in monolithic microwave integrated circuits (MMIC) has made widespread applications of microstrip and other planar transmission lines such as coplanar waveguide (CPW) and coupled microstrip on semiconductor substrate. In addition to interconnection or transmission line applications, this class of transmission lines can be employed as circuit elements such as phase shifter, voltage-tunable filter, and voltage-controlled attenuator [1,2,3].

These applications are made possible by slow-wave propagation resulting from electron-electromagnetic interaction with the lossy semiconductor material. The device was experimentally studied with metal-insulator-semiconductor (MIS) configurations and with Schottky contact microstrip or CPW structures [3,4,5,6]. These structures were also theoretically investigated by a number of techniques such as spectral domain analysis (SDA), mode-matching method and finite element method (FEM) [7,8,9,10] based on MIS or so-called layered models. However, practical semiconductor devices like Schottky contact microstrip or CPW are certainly not laminated structures.

Instead, they both have localized depletion regions on semiconductors. The effect of these localized depletion regions has not yet been discussed. It is plausible to contemplate that the layered model commonly used for the analysis may not correctly describe the actual field distributions in the structure with localized depletion regions.

In this paper the finite element method based on E_z -H_z formulation [9,11] is used for a variety of slow-wave structures which can be best described by the localized model. In conjunction with this study, use of higher order elements ,e.g. quadratic isoparametric elements,is discussed and results are presented.

CHAPTER 2 : the Localized Models

The localized depletion models for Schottky contact microstrip and CPW are illustrated in Figure 2.1 and Figure 2.2 respectively. By setting the conductivity in Region III of Figure 2.1 and that in region IV of Figure 2.2 to zero, the localized models will be reduced to the conventional MIS or layered models.

Obviously, the boundaries of the depletion region in actual devices are not straight lines but curved. Such curved boundaries can be found from solutions of a static Poisson's equation for a given bias condition. The present algorithm can then be applied to such geometry. However, the objective of the present paper is to study the effect of localization. The essential feature can be found without solving the structures with curved depletion boundaries. Therefore, the localized depletion region is assumed to be rectangular in shape.

Furthermore, there is also practical interest in the development of low loss slow-wave circuit elements. Schottky contacts for both center and ground strips of the CPW are assumed under the same DC bias conditions. It is found that the loss in this CPW structure can be less than the case where only the center conductor is a Schottky contact in the CPW.

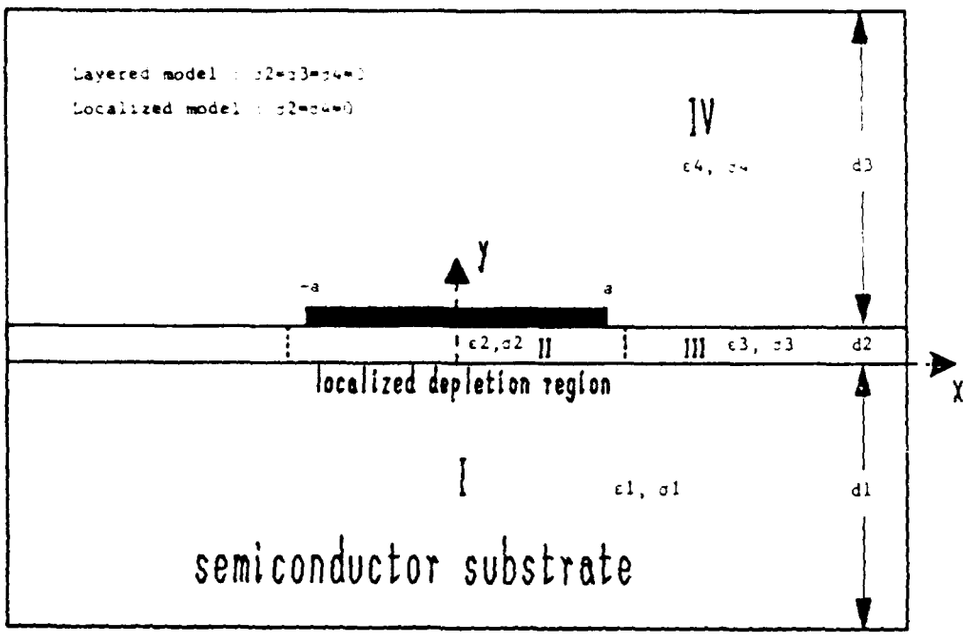

Figure 2.1 Localized depletion model for Schottky contact microstrip

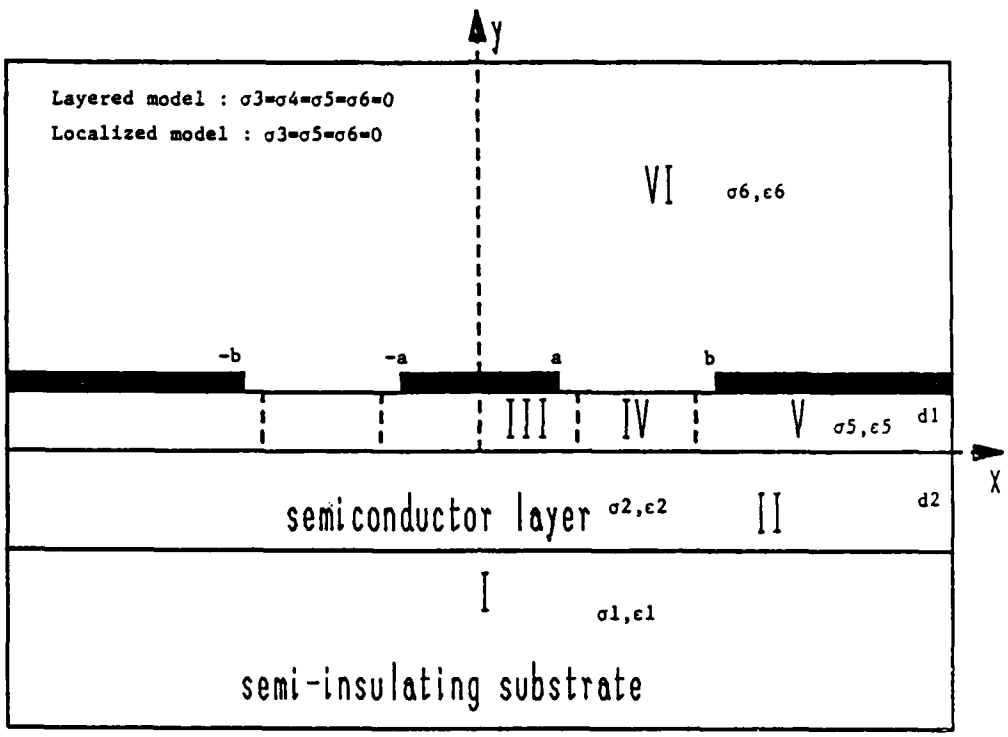

Figure 2.2 Localized depletion model for Schottky contact coplanar waveguide.

CHAPTER 3 : Derivation of the FEM Matrix Equation

A. Theory

The conventional E_z-H_z formulation that results in a homogeneous coupled symmetric matrix equation is adopted in this paper [9,11]. In the lossless case, the finite element method with E_z-H_z formulation provides a variational solution. The matrix equation can be derived by a functional followed by the Ritz approximation [11] or by weighted residual integration followed by the Galerkin's method [9] . It is possible to obtain a variational statement of the problem even for a lossy structure by dividing E_z and H_z components into real and imaginary parts [12]. Alternatively, the 3-vector H-formulation can be used [13,14]. This includes mixed boundary conditions and cautions must be exercised in treating the singularity at the corner of conductor edge. The conventional E_z-H_z formulation used here does not provide a variational solution for the lossy system. The method used here forces the residual to be zero by making it orthogonal to each member of a complete set of the trial functions. This method is one manifestation of the method of weighted residuals, which does not require the existence of a variational principle [15,16]. The method of weighted residuals

is not only simple for implementation, but, in principle, a systematic improvement on the accuracy of solution can be obtained if enough terms of the trial functions are used. In the part B of Chapter four, such improvements are discussed if one chooses quadratic elements instead of bi-linear elements in the lossy waveguide system.

B. Formulation

In a homogeneous, isotropic, linear waveguide with uniform cross-section, Figure 3.1, the Maxwell's equations can be represented by

$$(\nabla_t - \gamma \vec{U}_z) \times (\vec{E}_t + \vec{E}_z) = -j\omega\mu_e (\vec{H}_t + \vec{H}_z) \qquad (1)$$

$$(\nabla_t - \gamma \vec{U}_z) \times (\vec{H}_t + \vec{H}_z) = j\omega\varepsilon_e (\vec{E}_t + \vec{E}_z) \qquad (2)$$

Note that

1) $e^{j\omega t}$ and $e^{-\gamma z}$ factors are assumed for wave propagating along the positive z direction.

2) $\vec{E}=\vec{E}_t+\vec{E}_z$, $\vec{H}=\vec{H}_t+\vec{H}_z$; $\vec{E}_z=E_z\vec{U}_z$, $\vec{H}=H_z\vec{U}_z$

$\vec{U}_x$, $\vec{U}_y$, and $\vec{U}_z$ are unit vectors along x, y, and z direction, respectively.

3) $\nabla_t = \vec{U}_x \frac{\partial}{\partial x} + \vec{U}_y \frac{\partial}{\partial y}$

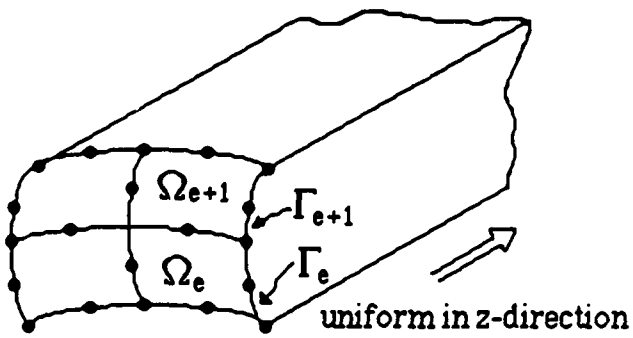

$$\Omega = \cdots \Omega_e \cup \Omega_{e+1} \cdots$$

Figure 3.1 A uniform waveguide discretized by eight-node quadratic elements

4) μ_o and ε_o are free space permeability and permittivity, while μ_{re} and ε_{re} are relative permeability and relative dielectric constant, respectively. Subscript e denotes element number e associated with subdomain Ω_e of the entire waveguide cross-section Ω which contains N_{ele} subdomains.

The equations (1) and (2) yield four equations:

$$\nabla_t x \vec{E}_z - \gamma \vec{U}_z x \vec{E}_t = -j\omega\mu_e \vec{H}_t \tag{3}$$

$$\nabla_t x \vec{E}_t = -j\omega\mu_e \vec{H}_z \tag{4}$$

$$\nabla_t x \vec{H}_z - \gamma \vec{U}_z x \vec{H}_t = j\omega\varepsilon_e \vec{E}_t \tag{5}$$

$$\nabla_t x \vec{H}_t = j\omega\varepsilon_e \vec{E}_z \tag{6}$$

Let the inner product be defined as

$$\langle \vec{R}, \vec{S} \rangle = \int_{\Omega_e} \vec{R} \cdot \vec{S} \, dxdy \tag{7}$$

,and the test functions

$\vec{P}=P\vec{U}_z$, P=0 on magnetic wall.

$\vec{Q}=Q\vec{U}_z$, Q=0 on electric wall.

,it can be shown from the equation (4) that

$$\langle \nabla_t \times \vec{E}_t, \vec{P} \rangle = -j\omega\mu_e \langle \vec{H}_z, \vec{P} \rangle$$

$$\langle \nabla_t \times \vec{E}_t, \vec{P} \rangle = \int_{\Gamma_e} \vec{n} \times \vec{E}_t \cdot \vec{P} ds + \langle \vec{E}_t, \nabla_t \times \vec{P} \rangle \qquad (8)$$

Since

(i) $\vec{n} \times \vec{E}_t = 0$ on electric wall.

(ii) $\int_{\Gamma_e} \vec{n} \times \vec{E}_t \cdot \vec{P} = 0$, $\vec{P}=0$ on agnetic wall.

(iii)

$$\int_{\Gamma_e} \vec{n}_1 \times \vec{E}_{t1} \cdot \vec{P} ds + \int_{\Gamma_{e+1}} \vec{n}_2 \times \vec{E}_{t2} \cdot \vec{P} ds$$

$$= \int_{\Gamma_e} (\vec{n}_1 \times \vec{E}_{t1} - \vec{n}_1 \times \vec{E}_{t2}) \cdot \vec{P} ds = 0$$

,it is concluded that

$$\sum_{e=1}^{Nele} \langle \nabla_t \times \vec{E}_t, \vec{P} \rangle = \sum_{e=1}^{Nele} \langle \vec{E}_t, \nabla_t \times \vec{P} \rangle \qquad (9)$$

Similarly, from the equation (6) one obtains

$$\sum_{e=1}^{Nele} \langle \nabla_t \times \vec{H}_t, \vec{Q} \rangle = \sum_{e=1}^{Nele} \langle \vec{H}_t, \nabla_t \times \vec{Q} \rangle \qquad (10)$$

The equations (3) and (5) can be reduced to

$$K_e^2 \vec{E}_t = -j\omega\mu_e(\nabla_t H_z)x\vec{U}_z - \gamma(\nabla_t E_z) \tag{11}$$

$$K_e^2 \vec{H}_t = j\omega\varepsilon_e(\nabla_t E_z)x\vec{U}_z - \gamma(\nabla_t H_z) \tag{12}$$

,where $K_e^2 = \omega^2\mu_e\varepsilon_e + \gamma^2$

Combine the equations (8), (9), and (11) to obtain

$$\sum_{e=1}^{Nele} \int_{\Omega_e} \frac{1}{K_e^2}[\mu_{re}(\nabla_t P)\cdot(\nabla_t U) + j\frac{\gamma C}{\omega}(\nabla_t P)x(\nabla_t V)\cdot\vec{U}_z]dxdy$$
$$= \sum_{e=1}^{Nele} \int_{\Omega_e} \mu_{re} U\cdot P \; dxdy \tag{13}$$

Similar to the derivation of the equation (13), the equations (6), (7), and (10) can be reduced to

$$\sum_{e=1}^{Nele} \int_{\Omega_e} \frac{1}{K_e^2}[\varepsilon_{re}(\nabla_t Q)\cdot(\nabla_t V) - j\frac{\gamma C}{\omega}(\nabla_t Q)x(\nabla_t U)\cdot\vec{U}_z]dxdy$$
$$= \sum_{e=1}^{Nele} \int_{\Omega_e} \varepsilon_{re} V\cdot Q \; dxdy \tag{14}$$

Note that the normalized variables are introduced.

$$U = \sqrt{\mu_o}Hz, \quad V = \sqrt{\varepsilon_o}E_z, \quad C = \frac{1}{\sqrt{\mu_o\varepsilon_o}}$$

The variables U, V and the test functions P, Q are then expanded in the following way:

$$U(x,y) = \sum_{j=1}^{N} U_j W_{jm} \tag{15}$$

$$V(x,y) = \sum_{j=1}^{N} V_j W_{je} \tag{16}$$

, where W_{jm} and W_{je} are shape functions at j-th node. N is the total number of nodes. $U_r=0$ if the r-th node is on the magnetic wall and $U_s=0$ if the s-th node is on the electric wall.

$$P(x,y) = \sum_{i=1}^{N} P_i W_{im} \tag{17}$$

$$Q(x,y) = \sum_{i=1}^{N} Q_i W_{ie} \tag{18}$$

,where $W_{im}(x_r,y_r)=0$ for i=1,N if the r-th node is on the magnetic wall, and $W_{ie}(x_s,y_s)=0$ for i=1,N if the s-th node is on the electric wall.

The final FEM homogeneous matrix equations are obtained by substituting the equations (15) through (18) into the equations (13) and (14).

$$\underset{\sim}{P}^T \underset{\approx}{K}(1) \underset{\sim}{U} + \underset{\sim}{P}^T \underset{\approx}{K}(2) \underset{\sim}{V} = 0 \tag{19}$$

$$\underset{\sim}{Q}^T \underset{\approx}{K}(3) \underset{\sim}{U} + \underset{\sim}{Q}^T \underset{\approx}{K}(4) \underset{\sim}{V} = 0 \tag{20}$$

,where

$$\underset{\sim}{P} = \begin{bmatrix} P_1 \\ P_2 \\ \vdots \\ P_N \end{bmatrix} \quad , \underset{\sim}{Q} = \begin{bmatrix} Q_1 \\ Q_2 \\ \vdots \\ Q_N \end{bmatrix} \quad , \underset{\sim}{U} = \begin{bmatrix} U_1 \\ U_2 \\ \vdots \\ U_N \end{bmatrix} \quad , \underset{\sim}{V} = \begin{bmatrix} V_1 \\ V_2 \\ \vdots \\ V_N \end{bmatrix}$$

$$\underset{\approx}{K}^{(1)}_{NxN} = \int_{\Omega_h} \left[\frac{\mu_{re}}{K_e^2} (\nabla_t W_{im}) \cdot (\nabla_t W_{jm}) - \mu_{re} W_{im} W_{jm} \right] dxdy$$

$$\underset{\approx}{K}^{(2)}_{NxN} = \int_{\Omega_h} \frac{+j\gamma C}{\omega K_e^2} \nabla_t W_{im} \times \nabla_t W_{je} \, dxdy$$

$$\underset{\approx}{K}^{(3)}_{NxN} = \int_{\Omega_h} \frac{-j\gamma C}{\omega K_e^2} \nabla_t W_{ie} \times \nabla_t W_{jm} dxdy = \left[K^{(2)}_{NxN} \right]^T$$

$$\underset{\approx}{K}^{(4)}_{NxN} = \int_{\Omega_h} \left[\frac{\varepsilon_{re}}{K_e^2} (\nabla_t W_{ie}) \cdot (\nabla_t W_{je}) - \varepsilon_{re} W_{ie} W_{je} \right] dxdy$$

The equation (20) can be written in a compact form.

$$[\underset{\sim}{P}^T \; \underset{\sim}{Q}^T] \begin{bmatrix} \underset{\approx}{K}^{(1)} & \underset{\approx}{K}^{(2)} \\ \underset{\approx}{K}^{(3)} & \underset{\approx}{K}^{(4)} \end{bmatrix} \begin{bmatrix} \underset{\sim}{U} \\ \underset{\sim}{V} \end{bmatrix} = 0 \qquad (21)$$

Since the test function functions P and Q are arbitrary, the equation (21) can be reduced to

$$A\,X = 0 \tag{22}$$

,where

$$A = \begin{bmatrix} \underset{\approx}{K}^{(1)} & \underset{\approx}{K}^{(2)} \\ \underset{\approx}{K}^{(3)} & \underset{\approx}{K}^{(4)} \end{bmatrix} \qquad X = \begin{bmatrix} \underset{\sim}{U} \\ \underset{\sim}{V} \end{bmatrix}$$

For a non-trival solution of X, det(A) must be zero.

C. Application of the Finite Element Method

The important steps in the actual coding of the final matrix equation obtained can he found in [17]. The hierarchy of the program can accept any isoparametric elements. In the present paper, four-node bi-linear and quadratic eight-node elements are used. The four-node element has complete linear polynomials along its boundary, and the eight-node element has complete quadratics.

Their differences in terms of numerical results will be discussed.

By alternating E_z and H_z nodal variables in the column vector X, the matrix A becomes a banded matrix. Finally, rows and columns corresponding to the Dirichlet boundary conditions are deleted such that E_z and H_z vanish at electric and magnetic walls, respectively. Therefore, the matrix A has dimension MxM, where M equals (2N-L). N is the total number of nodes and L stands for the sum of the total number of nodes located on electric or magnetic walls. The complex root of the equation, det(A)=0, is the solution for the propagation constant. The real and imaginary parts of the propagation constant correspond to the attenuation constant and the slow-wave factor, respectively.

CHAPTER 4 : Numerical Results

A. Validity Check

The present FEM code was applied to lossless printed line structures and excellent agreement obtained with the available data such as Fig.2.7 and Fig.7.11 in [18]. For the lossy layered case, Figure 4.1 and Figure 4.2 compare the results obtained by the present method as applied to a layered structure and other existing data for MIS CPW slow-wave propagation both theoretically and experimentally. The small discrepancy among various methods may be attributed to the CPW structure which has relatively high aspect ratio (b/a), i.e. 10, and very thin insulating region. None of the numerical solutions can find very accurate answers over the frequency span of interest. In particular, it is well known that the slender element, which is very long on one side and very short on the other side, may yield poor accuracies in the FEM analysis of a physical problem [19]. Owing to the fact that either the depletion or the lossy semiconductor region is extremely thin, it is inevitable that slender elements exist if the use of higher order and finer elements is not incorporated in the FEM. Therefore, quadratic 8-node elements and total number of 96 nodes are used for this

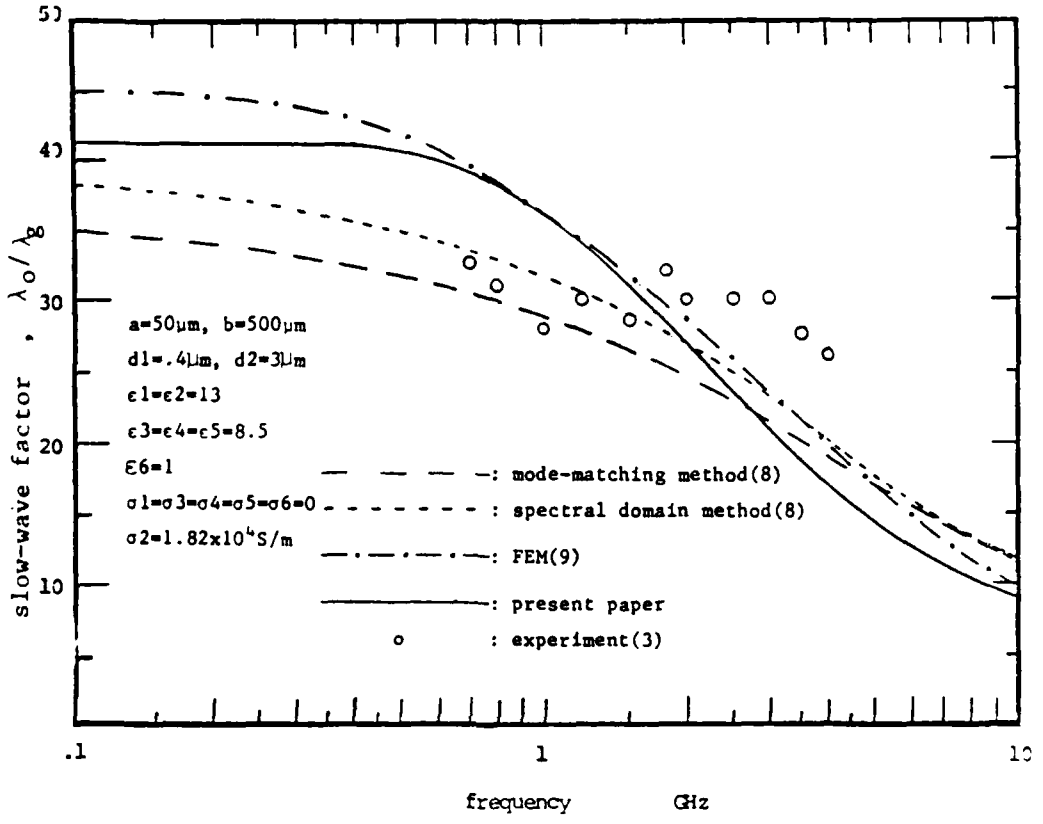

Figure 4.1 Plots of the slow-wave factor obtained by the present paper and other theories such as mode matching method [8], SDA [8], and FEM [9] together with experimental data [3] for an MIS CPW with dimensions shown in the figure.

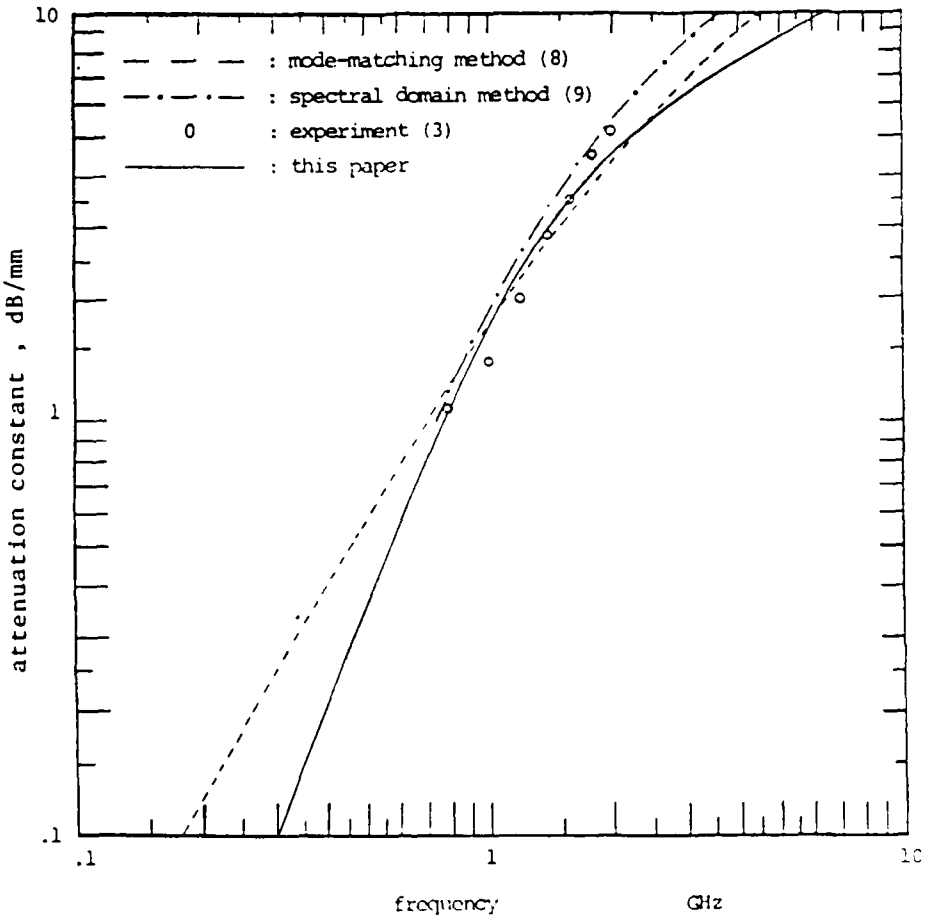

Figure 4.2 Plots of the attenuation constant obtained by the present paper and other theories such as mode-matching method [8], SDA [9], and FEM [9] together with experimental data for the MIS CPW analyzed in Figure 4.1.

particular structure.

The case for MIS microstrip slow-wave propagation is shown in Figures 4.3 and 4.4, where the discretization based on bi-linear elements and total number of 36 nodes is sufficient to match the data.

B. Bi-linear versus Quadratic Elements

Figures 4.5 and 4.6 compare computational results for slow-wave propagation in MIS microstrip model based on both bi-linear and quadratic elements. Both slow-wave factor and attenuation constant agree very well in low substrate conductivity, say less than .1 S/m.

When bi-linear elements are used, the slow-wave factor and attenuation constant approach infinity as substrate conductivity increases. Clearly this is non-physical, because very highly conducting substrate can be regarded as a metal layer and the slow-wave factor should be brought down when the substrate turns into metal. In fact, in the case of quadratic elements, the slow-wave factor starts to decline gradually and the attenuation constant(loss) starts to increase again when substrate

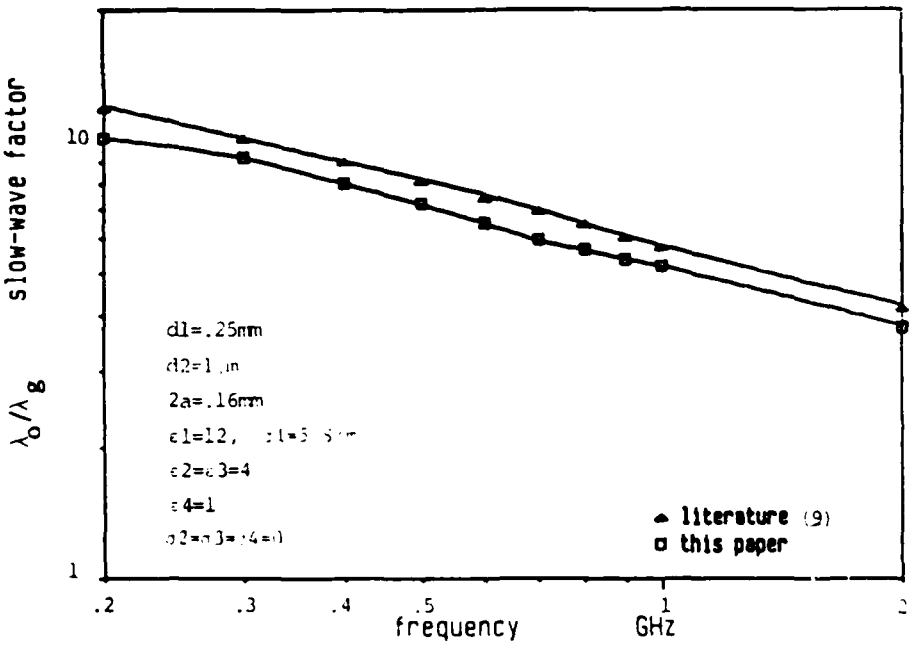

Figure 4.3 Validity check of the results obtained by this paper and the data in the literature [9]; the slow-wave factor versus frequency.

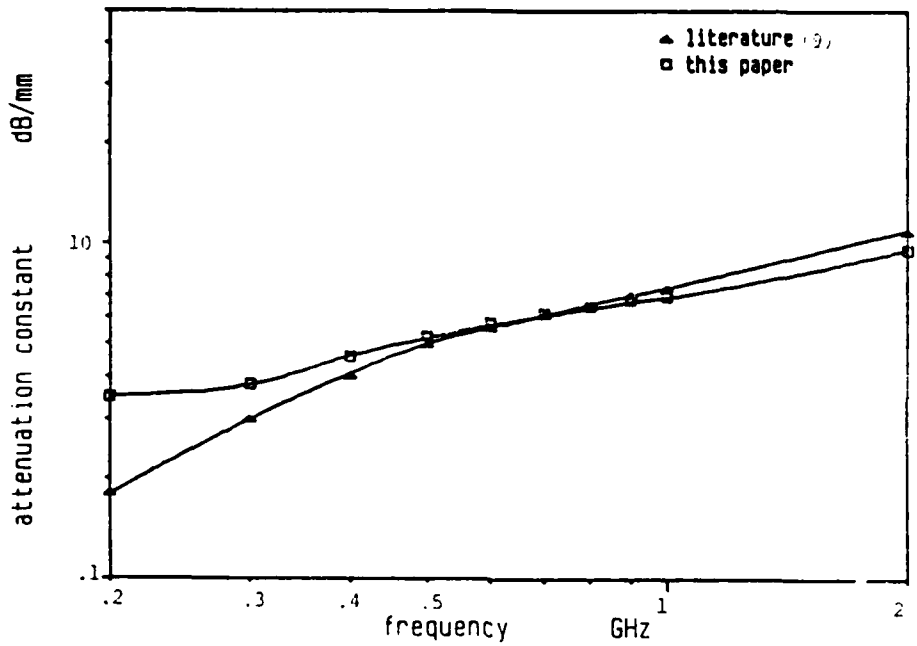

Figure 4.4 Validity check of the results obtained by this paper and data in the literature [9]; the attenuation constant versus frequency.

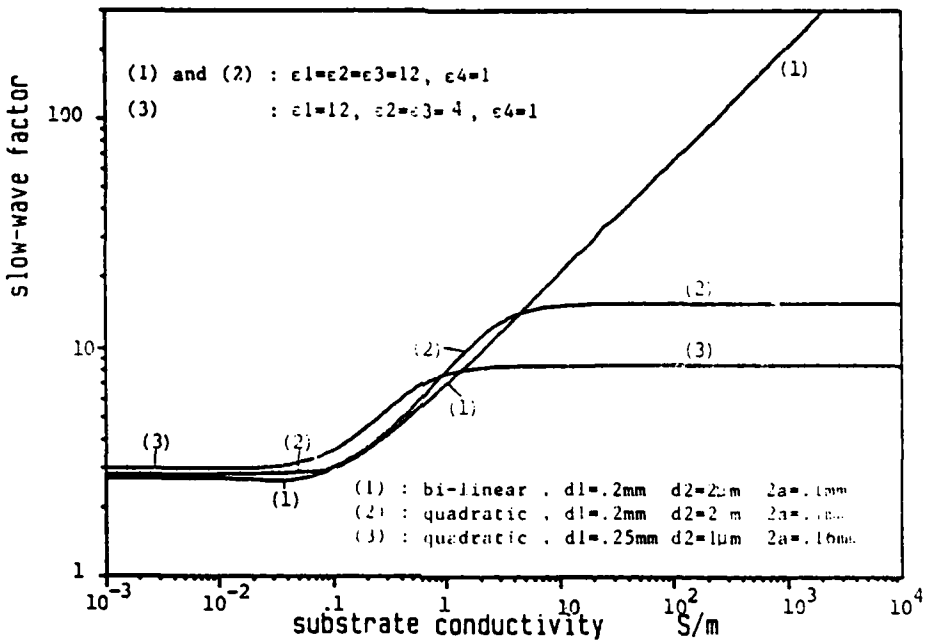

Figure 4.5 Comparisons of numerical results; the slow-wave factor versus substrate conductivity based on quadratic and bi-linear elements.

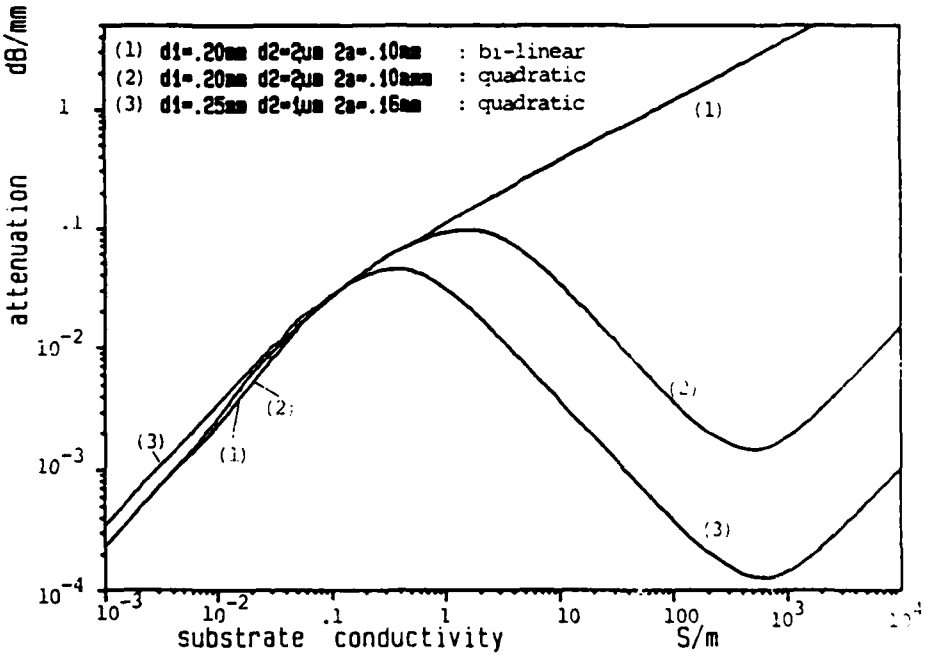

Figure 4.6 Comparison of numerical results; the attenuation constant versus microstrip substrate conductivity based on quadratic and bi-linear elements.

conductivity is increased from approximately 500 S/m. Similar comparative studies are performed for localized CPW models. The same phenomena that both slow-wave factor and attenuation constant approach infinity as the substrate conductivity increases are observed when bi-linear elements are employed.

Another type of comparative studies have been performed, i.e. numerical computations of the slow-wave factor and attenuation constant versus frequency by applying both bi-linear and quadratic elements on the same CPW structure. The results are illustrated in Figures 4.7 and 4.8. In these figures, curves based on quadratic elements are identical to those used in Figures 4.1 and 4.2. The solutions obtained by means of quadratic elements are apparently much closer to results obtained by other theoretical methods and experiments than those of linear elements. Additional studies on MIS microstrip also draw the same conclusion.

Since the accuracy of the quadratic elements is confirmed, the rest of the computations in the paper are based on quadratic elements except the results shown in Figures 4.9 and 4.10.

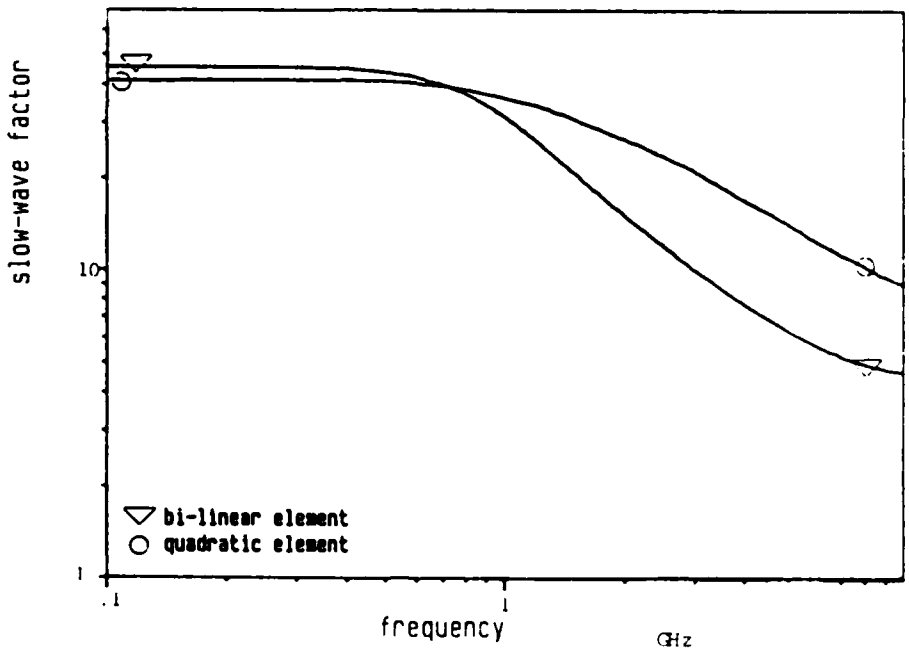

Figure 4.7 Comparison of numerical results, the slow-wave factor versus frequency on the same MIS CPW structure analyzed in Figures 4.1 and 4.2 based on quadratic and bi-linear elements.

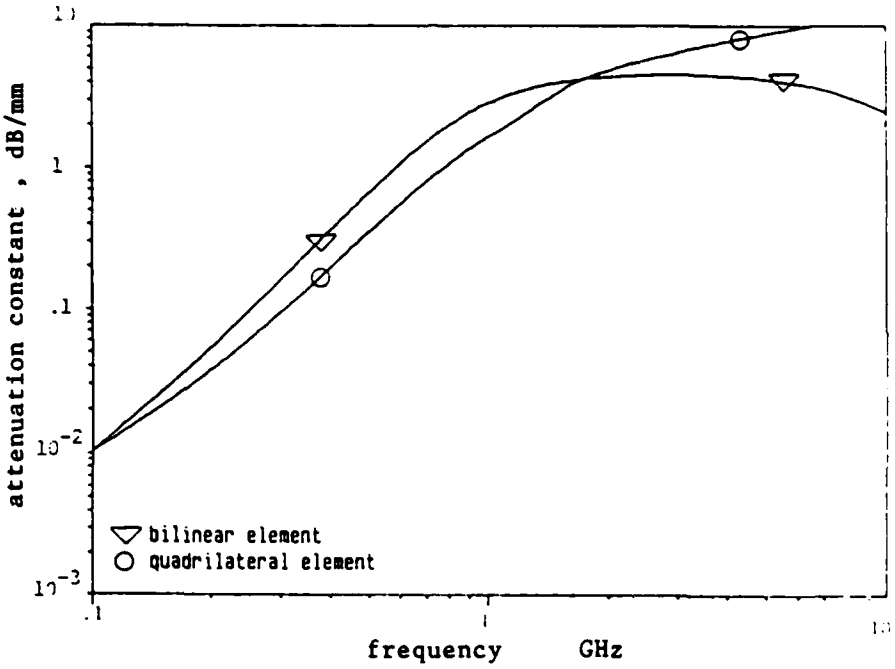

Figure 4.8 Comparison of numerical results, the attenuation constant versus frequency on the same MIS CPW structure analyzed in Figures 4.1 and 4.2 based on quadratic and bi-linear elements.

C. Effects of the Localized Depletion Regions on the Slow-Wave Propagation

It is clear in Figures 4.9 and 4.10 that the MIS layered model is a good model for microstrip slow-wave propagation. This conclusion is confirmed again using quadratic elements with improved accuracy. The solutions obtained by layered and localized models are very close and cannot be distinguished by plots. Table 4.1 shows how close the solutions are under different combinations of conductivities. For the localized CPW model, the results shown in Figures 4.11 and 4.12 are rather interesting. Two CPW's with various dimensions are syudied here. Structure (2) has about half the gap width, i.e. (b-a), to structure (1) and all the rest of the conditions are almost the same. The results indicated taht the conducting Region IV has a stronger influence on the structure (2). A noticeable transition region exists where the attenuation constant (loss) starts to decline and the slow-wave factor changes abruptly and settles quickly as σ_4 increases. The skin depth, which is inversely proportional to the square root of the conductivity, is relatively large in Region IV, approximately 50 mm for σ_4 = 0.1 S/m. Electromagnetic field penetrates Region IV freely and interacts with it in terms of lossy dielectric material. When σ_4

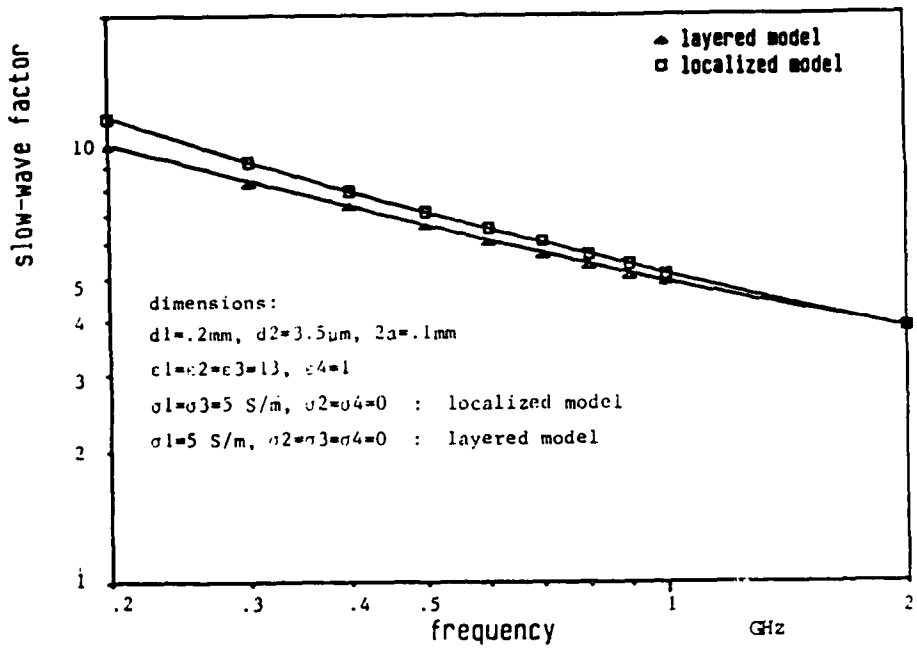

Figure 4.9 Comparison of plots of the slow-wave factor versus frequency based on localized and layered models for Schottky contact microstrips.

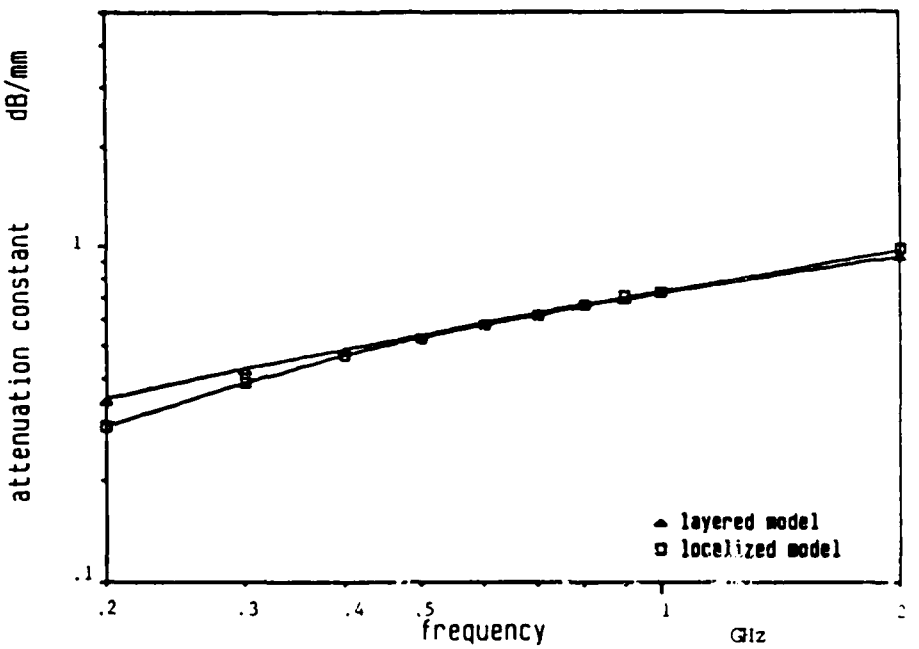

Figure 4.10 Comparison of plots of the attenuation constant versus frequency based on localized and layered models for Schottky contact microstrips.

(slow-wave factor, dB/mm)

MODEL	σ1(S/m) / σ3(S/m)	5	20×10^{3}
Layered	0	(8.364661, .0072815)	(8.397601, .0019445)
Localized	5	(8.391247, .0073026)	(8.397601, .0019502)
	20×10^{3}	(8.398345, .0067541)	(8.399383, .0019613)

conditions : a=80μm, d1=250μm, d2=1μm, ε1=12, ε2=ε3=4, ε4=1, μ2=μ4=0
(microstrip)
frequency=.1GHz

Table 4.1 Comparison of slow-wave propagations for layered and localized microstrip models.

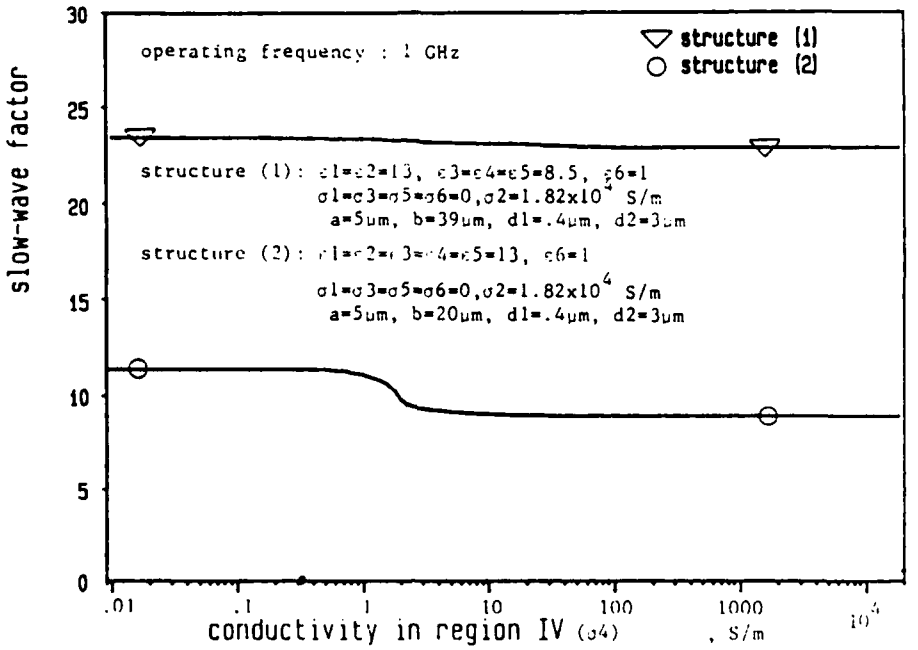

Figure 4.11 Effects of the localized depletion region on CPW's; the slow-wave factor versus the conductivity of the region four(IV) of Figure 2.2.

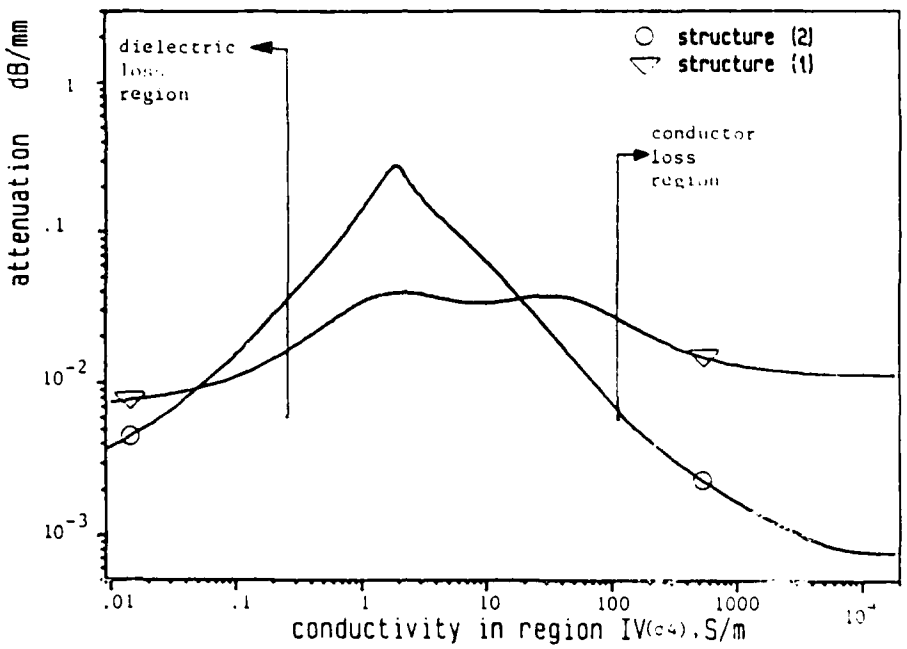

Figure 4.12 Effects of the localized depletion region on CPW's; the attenuation constant versus the conductivity of the region four(IV) of Figure 2.2.

is increased to 10^5 S/m the skin depth is reduced to 50 μm. This is very close to the gap widths in structures (1) and (2). As a result, the highly conducting Region IV can be in effect replaced by a piece of thin and imperfect metal inserted into the gap. The loss introduced at higher values of σ_4 is much more closely related to skin-effect ohmic loss. Generally speaking, the loss mechanism due to Region IV in the CPW structure can be separated into dielectric loss and conductor loss. The former increases as conductivity increases and the latter decreases as conductivity increases. Common waveguides and transmission lines also exhibit similar loss behavior [20].

Qualitative discussions can be readily extended to obtain an equivalent transmission line circuit representation of the localized CPW in Figure 4.13. This empirical model happens to be a slight modification of the analytical model of the Schottky contact coplanar line based on semi-empirical considerations and is indeed identical if we combine C_1 and C_3 into a single capacitor. Note that in the localized CPW structure, semiconductor Schottky contacts are under the metal strips. L_o and R_o represent the inductance and resistance due to ohmic loss and skin loss per unit length, respectively. C_o represents the capacitance per unit length between center and ground strips in

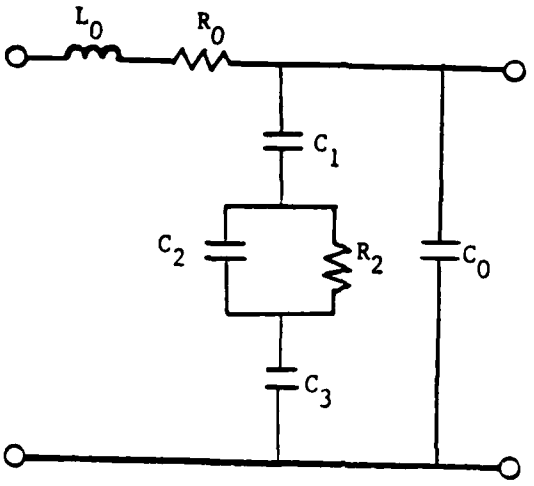

Figure 4.13 Approximate transmission line circuit representation of the Schottky contact CPW with localized depletion regions under metal strips.

Region VI. C_1 represents the capacitance per unit length from center strip to the edges of Region IV and Region II. C_3 represents the capacitance per unit length from the ground strip to the other side of the Region IV and the edge of Region II. Parallel R_2 and C_2 represent the circuit contributions of Region IV and part of Region II. General discussions leading to the determination of these component values can be found in [21,22].

Figures 4.14 and 4.15 compare numerical results obtained by layered and localized models for the slow-wave propagation on CPW's. The localized model tends to show better performance with more linear slow-wave characteristics versus frequency and less loss at higher frequency in the structure under analysis. It suggests that the structure with Schottky contacts for all metal strips, Figure 2.2, may become a practical slow-wave configuration.

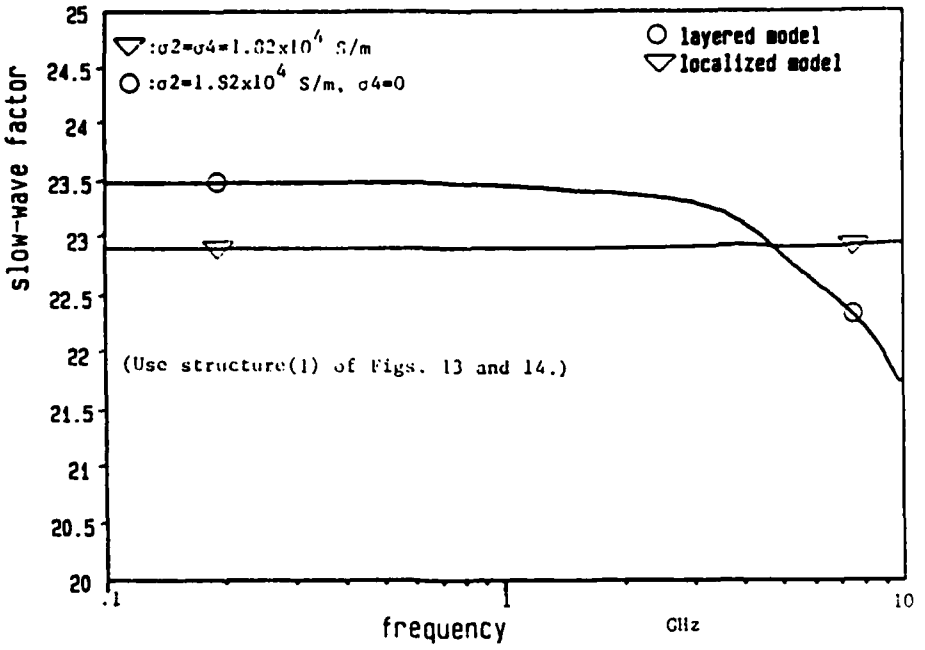

Figure 4.14 Comparison of plots of the slow-wave factor versus frequency based on localized and layered models for CPW's.

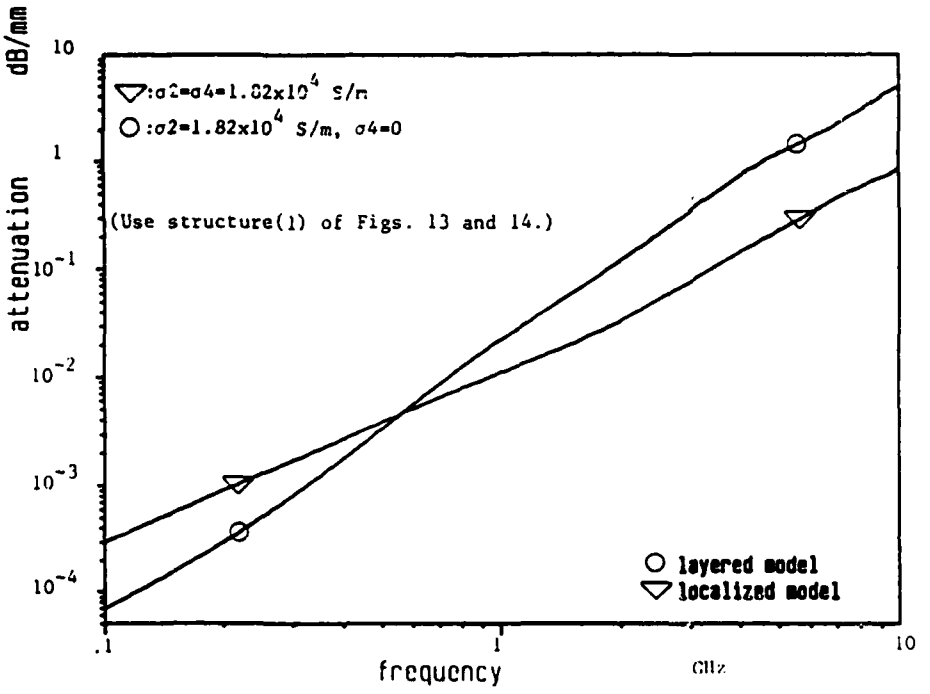

Figure 4.15 Comparison of plots of the attenuation constant versus frequency based on localized and layered models for CPW's.

CHAPTER 5 : Applications

Along with the study of the effects of the localized depletion models on MMIC slow-wave circuits a general purpose FEM program was developed for the analysis and design of planar waveguides. Figure 5.1 shows several possible applications among a broad class of MMIC waveguides that can be analyzed by extensions of the present code. These structures can not be modeled accurately by an MIS layered model. The results obtained from the analysis of CPW and microstrip MMIC's with localized models suggest that it is possible to tune the slow-wave circuit to meet certain design specifications by selective ion implantations on the locations proposed in Figure 5.1 with appropriate controls over doping concentration and geometry. A certain mode of propagation may be more subject to the existing selective ion-implanted regions than the other mode of propagation and the additional ion-implanted region can enhance or reduce the loss associated with it depending on what the doping profile is.

The FEM code can also be applied to analyze a variety of waveguides with non-uniform material propertities. These non-uniformities can be characterized by the input data with various

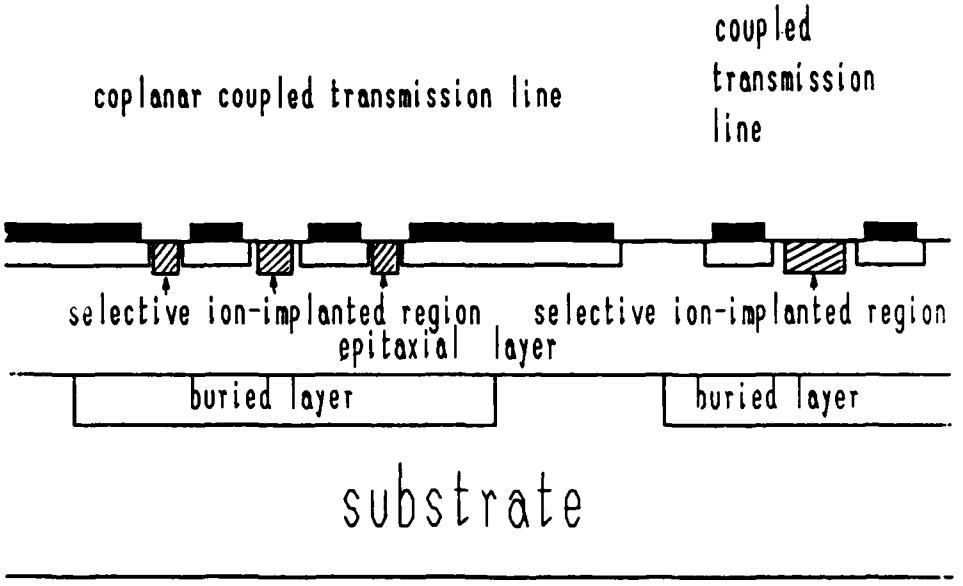

Figure 5.1 Potential applications of the extensions of the localized depletion models to MMIC planar waveguide designs, e.g. coupled coplanar lines and coupled lines with selective ion implantations which add more degrees of freedom to design slow-wave circuits.

material properties known at each specific node. For example, an optically controlled CPW phase shifter proposed by Cheung and Neikirk [23] has non-unifom carrier concentrations in the semiconducting region after optical injection. Such non-uniformities can be effectively analyzed by the FEM field analysis program.

CHAPTER 6 : Conclusions

Extensive computer simulations employing the FEM technique on CPW and microstrip MMIC slow-wave structures have been performed to study the differences on slow-wave propagations between layered models commonly used in the past and the localized model which is closer to the physical situation. The results show that the layered model is a good approximation for the microstrip case. On the other hand, the localized model yields more accurate solutions for Schottky CPW structures. It was also pointed out that higher order elements improve solutions for the geometry under analysis. The work can be extended to analyze and design more complicated planar waveguides.

References

[1] K. Frike and H. L. Hartnagel,'GaAs MESFET Optimization and new Device Applications based on Wave Property Studies,' IEEE MTT-S International Microwave Symposium, pp.192-195, June 1985.

[2] C. Seguinot, P. Kennis, P. Pribetich, and J. F. Legier,'Performances Prediction of an Ultra Broad-Band Voltage-Controlled Attenuator Using Schottky Contact Coplanar Line Properties,' IEEE Electron Device Letters, Vol. EDL-7, No. 2, February 1986.

[3] H. Hasegawa and H. Okizaki,'M.I.S. and Schottky slow-wave coplanar stripline on GaAs substrates,' Electron. Lett., vol. 13, pp.663-664, Oct. 1977.

[4] H. Hasegawa, M. Furukawa, and H. Yanai,'Properties of microstriplines on Si-SiO_2 system,' IEEE Trans. Microwave Theory Tech. vol. MTT-19, pp.869-881, Nov. 1971.

[5] D. Jager,'Slow-wave propagation along variable Schottky-contact microstrip line,' IEEE Trans. Microwave Theory and Tech., vol. MTT-24, pp.566-573, Sept. 1976.

[6] D. Jager and W. Rabus,'Bias dependent phase delay of Schottky-contact microstrip line,' Electron. Lett., vol.9, no.9,pp.201-203, 1973.

[7] Y.C. Shih and T. Itoh,'Analysis of printed transmission lines for monolithic integrated circuits,' Electron. Lett., vol.18, no.14, pp.585-586, July 1982.

[8] Y. Fukuoka, Y. C. Shih, and T. Itoh,'Analysis of slow-wave coplanar waveguide for monolithic integrated circuits,' IEEE Trans. Microwave Theory and Tech., vol. MTT-31, no.7, pp.567-573, July 1983.

[9] M. Aubourg, J. P. Villotte, F. Goon, and Y. Grault,'Analysis of M.I.S. or Schottky contact coplanar lines using the F.E.M. and S.D.A.,' IEEE MTT-S International Microwave Symposium, pp.396-398, June 1983.

[10] R. Sorrentino, G. Leuzzi, and A. Silbermann,'Characteristics of metal-insulator-semiconductor coplanar waveguides for monolithic microwave circuits,' IEEE Trans. Microwave Theory and Tech., vol. MTT-32, no.4, pp.410-416, April 1984.

[11] P. Daly,'Hybrid-mode analysis of microstrip by finite element methods,' IEEE Trans. Microwave Theory and Tech., vol. MTT-19, no.1, pp.19-25, Jan. 1971.

[12] A. D. McAulay,'Variational finite-element solution for dissipative waveguides and transportation application,' IEEE Trans. Microwave Theory and Tech., vol. MTT-25, no. 5, pp.382-392, May 1977.

[13] S. R. Cvetkovic and J. B. Davies,'Self-adjoint vector

variational formulation for lossy anisotropic dielectric waveguide,' IEEE Trans. Microwave Theory and Tech., vol. MTT-34, no.1, pp.129-134, Jan. 1986.

[14] C. H. Chen and C. Lien,'The variational principle for non-self-adjoint electromagnetic problems,' IEEE Trnas. Microwave Theory and Tech., vol. MTT-28, no. 8, pp.878-886, August 1980.

[15] A. K. Noor,'Multifield(mixed and hybrid) finite element model,' pp.127-156, Ch.5, State-of-the-Art Surveys on Finite Element Technology , 1983.

[16] B. A. Finlayson, The Method of Weighted Residuals and Variational Principles, Academic Press, 1972.

[17] E. B. Becker, G. F. Carey, and J. T. Oden, Finite Elements, vol.I, Prentice-Hall, Inc., New Jersey, 1981.

[18] K. C. Gupta, R. Garg, I. J. Bahl, Microstrip Lines and Slot Lines, Artech House, Inc., Massachusetts, 1979.

[19] G. F. Carey and J. T. Oden, Finite Elements, vol. II, Prentice-Hall, Inc., New Jersey, 1983.

[20] S. Ramo, J. R. Whinnery, T. V. Duzer, Fields and Waves in Communication Electronics, John Wiley & Sons, 1965.

[21] C. Seguinot, P. Kennis, P. Pribetich, J. F. Legier, 'Analytical model of the Schottky contact coplanar line,' Proc. 14th European Microwave conf., pp.160-165, Sep. 1984.

[22] H. Hasegawa, S. Seki, 'Analysis of Interconnection delay on very high-speed LSI/VLSI chips using an MIS microstrip line model,' IEEE Trans. Microwave Theory and Tech., vol. MTT-32, no.12, pp.1721-1727 December 1984.

[23] P. Cheung, D. Fun, D. Miller, C-K Tzuang, D. P. Neikirk, and T. Itoh,'Optically controlled coplanar waveguide millimeter wave phase-shifter,'Proceedings of the 10th International Conference on Infrared and Millimeter Waves, 1985.

CURITY CLASSIFICATION OF THIS PAGE

REPORT DOCUMENTATION PAGE

a. REPORT SECURITY CLASSIFICATION: UNCLASSIFIED	1b. RESTRICTIVE MARKINGS: AD-A179859
b. SECURITY CLASSIFICATION AUTHORITY	3. DISTRIBUTION / AVAILABILITY OF REPORT
b. DECLASSIFICATION / DOWNGRADING SCHEDULE	unlimited
4. PERFORMING ORGANIZATION REPORT NUMBER(S): Microwave Laboratory Report No. 87-P-2	5. MONITORING ORGANIZATION REPORT NUMBER(S): AFOSR-TR- 87-0481
6a. NAME OF PERFORMING ORGANIZATION: University of Texas; 6b. OFFICE SYMBOL (If applicable)	7a. NAME OF MONITORING ORGANIZATION
6c. ADDRESS (City, State, and ZIP Code): Department of Electrical & Computer Engineering, University of Texas, Austin, TX 78712	7b. ADDRESS (City, State, and ZIP Code)
8a. NAME OF FUNDING / SPONSORING ORGANIZATION: AFOSRINE; 8b. OFFICE SYMBOL (If applicable)	9. PROCUREMENT INSTRUMENT IDENTIFICATION NUMBER: AFOSR-86-0036
8c. ADDRESS (City, State, and ZIP Code): Building 410, Bolling AFB, DC 20332-6448	10. SOURCE OF FUNDING NUMBERS: PROGRAM ELEMENT NO. 61102F; PROJECT NO. 2305; TASK NO. C 1; WORK UNIT ACCESSION NO.

11. TITLE (Include Security Classification)

FINITE ELEMENT ANALYSIS OF SLOW-WAVE SCHOTTKY CONTACT PRINTED LINES

12. PERSONAL AUTHOR(S)

CHING-KUANG C. TZUANG, DEAN P. NEIKIRK AND TATSUO ITOH

13a. TYPE OF REPORT	13b. TIME COVERED	14. DATE OF REPORT (Year, Month, Day)	15. PAGE COUNT
technical report	FROM ____ TO ____	Feb. 16, 1987	45

16. SUPPLEMENTARY NOTATION

17. COSATI CODES			18. SUBJECT TERMS (Continue on reverse if necessary and identify by block number)
FIELD	GROUP	SUB-GROUP	

19. ABSTRACT (Continue on reverse if necessary and identify by block number)

Extensive finite element analyses on MMIC (monolithic microwave integrated circuit) slow-wave structures with both localized and layered models are presented. Good agreement is achieved for results obtained in this paper with other theoretical results and experiments. Higher order elements that improve accuracy are discussed. The comparative studies for the Schottky contact microstrip and the coplanar waveguide with localized and layered models are presented. Potential applications of the localized models to more general and practical slow-wave circuits are also discussed.

20. DISTRIBUTION / AVAILABILITY OF ABSTRACT	21. ABSTRACT SECURITY CLASSIFICATION
☒ UNCLASSIFIED/UNLIMITED ☐ SAME AS RPT ☐ DTIC USERS	
22a. NAME OF RESPONSIBLE INDIVIDUAL	22b. TELEPHONE (Include Area Code) / 22c. OFFICE SYMBOL

D FORM 1473, 84 MAR — 83 APR edition may be used until exhausted. All other editions are obsolete. SECURITY CLASSIFICATION OF THIS PAGE